

## BIPOLAR CLUMP EJECTION FROM A MOVING SOURCE

J. Cantó,<sup>1</sup> A. C. Raga,<sup>2</sup> L. Loinard,<sup>3</sup> and L. F. Rodríguez<sup>3</sup>

Received 2008 June 26; accepted 2008 August 6

### RESUMEN

Presentamos un modelo para una eyección bipolar de dos nubes de una fuente que viaja dentro de un medio homogéneo. El modelo tiene una solución analítica completa, de la cual derivamos parámetros que pueden ser comparados directamente con observaciones (por ejemplo, la orientación de la línea que une a las dos nubes y la separación entre las nubes en función del tiempo). Comparamos el modelo analítico con una simulación 3D (con una función de enfriamiento parametrizada), y encontramos que las posiciones de las nubes obtenidas del modelo analítico coinciden relativamente bien con los resultados de la simulación numérica.

### ABSTRACT

We present a model for the bipolar ejection of clumps from a source traveling within the surrounding, homogeneous ambient medium. The model has a full analytic solution, from which we derive parameters which can be directly compared with observations (e. g., the orientation of the line joining the two clumps and the separation between the clumps as a function of time). We compare the analytic model with a full 3D numerical simulation (with a parametrized cooling function), and find that the positions of the clumps obtained from the analytic model agree relatively well with the results from the numerical simulation.

*Key Words:* ISM: jets and outflows — ISM: kinematics and dynamics — stars: pre-main sequence — stars: mass loss

### 1. INTRODUCTION

A number of bipolar Herbig-Haro (HH) jets show curved structures, which apparently are the result of a relative motion between the star which ejects them and the surrounding environment. Clear examples of this kind of object are the jets discovered in the periphery of photoionized regions by Bally & Reipurth (2001). Another good example of this situation is provided by the outflow from PV Cep (Goodman & Arce 2004), an object embedded in a neutral region.

There has been a substantial amount of theoretical work on the interaction of an HH jet with a sidewind. Cantó & Raga (1995) developed an analytic model which gives the curved shape of a steady jet interacting with a sidewind. This model was compared with 3D HH jet simulations by Lim & Raga (1998). Masciadri & Raga (2001) presented 3D sim-

ulations of variable HH jets in a sidewind, with the purpose of modelling the photoionized jets of Bally & Reipurth (2001). Finally, Ciardi et al. (2008) presented both 3D simulations of HH jets (with a constant ejection) and a laboratory experiment of a jet in a sidewind.

The simulations of Masciadri & Raga (2001) show that internal working surfaces produced by a low amplitude ejection velocity variability follow trajectories that approximately coincide with the locus of the curved jet beam. On the other hand, the leading head of the jet follows a straighter trajectory, which detaches from the curved jet beam. This effect was also found by Ciardi et al. (2008).

In other words, we have two possible behaviors:

1. Small working surfaces (due to low amplitude ejection velocity variabilities) travel along the path of the “jet/sidewind” model of Cantó & Raga (1995),
2. Large working surfaces (resulting from the “turning on” of the jet or from large amplitude ejection velocity variabilities) detach from

<sup>1</sup>Instituto de Astronomía, Universidad Nacional Autónoma de México, Mexico.

<sup>2</sup>Instituto de Ciencias Nucleares, Universidad Nacional Autónoma de México, Mexico.

<sup>3</sup>Centro de Radioastronomía y Astrofísica, Universidad Nacional Autónoma de México, Morelia, Mexico.

the curved jet beam, and follow somewhat straighter trajectories.

The present paper describes an analytic model and numerical simulations of the latter situation, in which we have working surfaces which become detached clumps, and travel into the sidewind as individual “bullets”. The models we present of course also apply for the case in which an outflow source (travelling within the surrounding medium) has discrete, bipolar “ejection events”.

The paper is organized as follows. In § 2, we present an analytic model for a bipolar clump ejection from a source in motion with respect to the surrounding environment. In § 3 we present 3D numerical simulations of the same problem, and carry out a comparison between the numerical results and the analytic model. Finally, we present a discussion of the results in § 4.

## 2. THE ANALYTIC MODEL

An outflow source moves with a constant velocity  $v_*$  along the  $x$ -axis of a reference frame in which the surrounding ISM is stationary. At  $t = 0$ , the outflow source is at the origin of this reference frame, and after a time  $\tau$  it is located at a position

$$x_0 = v_*\tau, \quad (1)$$

along the  $x$ -axis, as shown in Figure 1. At  $t = \tau$ , the outflow source ejects a clump of mass  $M$  at a velocity  $v_e$ , at an angle  $\beta$  with respect to the  $x$ -axis, where both  $v_e$  and  $\beta$  are measured in a reference frame that moves with the outflow source (with an abscissa which is parallel to the  $x$ -axis of the stationary system). The  $y$ -axis of the stationary coordinate system is defined so that the vector velocity  $\bar{v}_e$  (with which the clump is ejected) lies on the  $xy$ -plane. Then, the ejection velocity vector measured in the stationary reference frame (i. e., the frame in which the ISM is at rest) is

$$\bar{v}_0 = (v_* + v_e \cos \beta) \hat{e}_x + v_e \sin \beta \hat{e}_y, \quad (2)$$

which has a modulus

$$v_0 = (v_*^2 + v_e^2 + 2v_*v_e \cos \beta)^{1/2}. \quad (3)$$

In the stationary frame, after the ejection the clump moves in a straight line along the  $s$ -axis (i.e., the direction of  $\bar{v}_0$ , see Figure 1). The angle  $\theta$  between the  $s$ -axis and the  $x$ -axis is given by

$$\tan \theta = \frac{v_e \sin \beta}{v_* + v_e \cos \beta}, \quad (4)$$

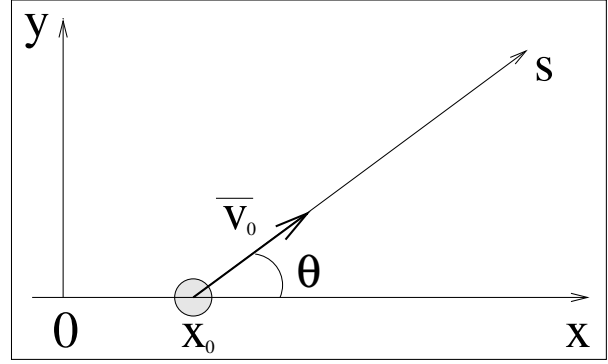


Fig. 1. Schematic diagram showing the parameters of the ejection of a clump from a source in motion along the  $x$ -axis of a reference system at rest with respect to the surrounding environment. At  $t = \tau$ , the source is at position  $x_0$  and ejects a clump along the  $\hat{s}$ -direction. The ejection direction lies on the  $xy$ -plane, and makes an angle  $\theta$  with respect to the  $x$ -axis.

where  $v_e$  and  $\beta$  are the modulus and the direction (respectively) of the ejection measured in a system moving with the outflow source (see above).

The clump moves in a straight line (in the stationary reference frame), but its velocity decreases due to the interaction with the surrounding, stationary medium. We now assume that the surrounding ISM has a uniform density  $\rho_0$ . Then its velocity is given by (see De Young & Axford 1967 and Cabrit & Raga 2000)

$$v(s) = v_0 \left(1 - \frac{s}{s_0}\right)^{3/4}, \quad (5)$$

where

$$s_0 \equiv \frac{3}{4} \left(\frac{Mv_0^4}{\xi\rho_0c^4}\right)^{1/3}, \quad (6)$$

$M$  is the mass of the clump,  $c$  the isothermal sound speed (of the clump material), and  $\xi = 14$  (see Cantó et al. 1998) is a constant that is obtained by integrating the drag force over the surface of the cometary clump.

Equation (5) can be integrated to obtain

$$s = s_0 \left\{ 1 - \left[ 1 - \frac{(t - \tau)}{t_0} \right]^4 \right\}, \quad (7)$$

where

$$t_0 \equiv \frac{4s_0}{v_0}. \quad (8)$$

From equations (5) and (7) it follows that the clump stops at a distance  $s_0$ , at a time  $t_0$  after ejection (see also De Young & Axford 1967).

The position of the clump in the stationary frame after a time  $t$  (see Figure 1) is

$$x = x_0 + s \cos \theta, \quad (9)$$

$$y = s \sin \theta, \quad (10)$$

where  $s$  is given by equation (7). At time  $t$ , the outflow source is at a position

$$x_* = v_* t, \quad (11)$$

$$y_* = 0. \quad (12)$$

Therefore, the coordinates of the clump with respect to a reference frame fixed to the outflow source are

$$\Delta x = x - x_* = -(t - \tau)v_* + s \cos \theta, \quad (13)$$

$$\Delta y = y - y_* = s \sin \theta. \quad (14)$$

The path followed by the clump in the reference frame of the outflow source can be found by combining equations (13) and (14), and eliminating the time using (7). One then obtains

$$\Delta x = \frac{\Delta y}{\tan \theta} - 4s_0 \left( \frac{v_*}{v_0} \right) \left[ 1 - \left( 1 - \frac{\Delta y}{s_0 \sin \theta} \right)^{1/4} \right]. \quad (15)$$

In order to illustrate the characteristics of this solution, we consider the problem of a source which simultaneously ejects two identical “bullets” at a time  $\tau = 0$ , the first one at an angle  $\beta_1$  with respect to the direction of motion of the outflow source (measured in the reference frame moving with the source), and the second one at an angle  $\beta_2 = \pi + \beta_1$ . We then choose a value for  $\beta_1$ , and a value for the ratio  $v_e/v_*$  between the ejection velocity and the velocity of the outflow source (with respect to the surrounding environment). We then use equation (4) to calculate the angles  $\theta_1$  and  $\theta_2$  (in the stationary reference frame, corresponding to the ejection angles  $\beta_1$  and  $\beta_2$ ), and use equation (15) to calculate the trajectories of the two clumps (in the reference frame moving with the outflow source).

The results obtained for  $v_*/v_e = 0.2, 0.5$  and  $0.8$ , and  $\beta_1 = 20, 45, 70$  and  $90^\circ$  are shown in Figure 2. In this figure, we also show the positions of the clumps at times  $t = 0$  (when they coincide with the position of the outflow source, at the origin of the  $\Delta x, \Delta y$  coordinate system), and at successive intervals  $\Delta\tau = 0.5s_1/v_e$  (where  $s_1$  is calculated setting  $\beta = \beta_1$  in equations 3 and 6).

In this figure, we see that the two clumps first travel away from the source in the direction  $\beta_1$  and  $\beta_2 = \pi + \beta_1$ , and that their trajectories curve until

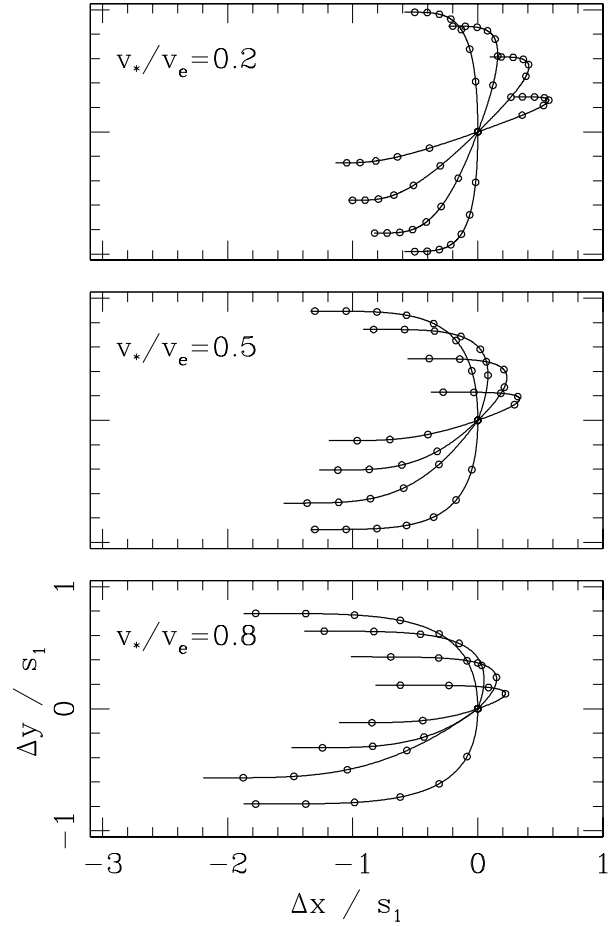


Fig. 2. Trajectories for bipolar clump ejections with  $v_*/v_e = 0.2$  (top),  $0.5$  (center) and  $0.8$  (bottom) in a reference system moving with the outflow source. In each frame, we show the trajectories for  $\beta_1 = 20, 45, 70$  and  $90^\circ$ . The solid circles correspond to the positions of the clouds at time-intervals  $\Delta t = 0.5s_1/v_e$ . The offsets  $\Delta x, \Delta y$  from the position of the outflow source are given in units of  $s_1$  (see the text).

they become parallel to the  $-\Delta x$ -axis. The trajectories shown in Figure 2 stop at the points in which the clumps become stationary with respect to the surrounding environment.

From observations of a bipolar clump ejection it is of course straightforward to calculate the mean position of the two observed clumps:

$$\Delta x_m = \frac{\Delta x_1 + \Delta x_2}{2}; \quad \Delta y_m = \frac{\Delta y_1 + \Delta y_2}{2}, \quad (16)$$

where the subscripts 1 and 2 refer to the two observed clumps; the orientation angle is

$$\alpha = \tan^{-1} \left( \frac{\Delta y_2 - \Delta y_1}{\Delta x_2 - \Delta x_1} \right), \quad (17)$$

and the distance between the two clumps is

$$d = \sqrt{(\Delta x_2 - \Delta x_1)^2 + (\Delta y_2 - \Delta y_1)^2}. \quad (18)$$

The determination of these quantities from the observations requires a knowledge of the orientation of the outflow with respect to the plane of the sky, which in principle can be obtained from proper motion and radial velocity measurements.

From our model, it is possible to show that to first order in  $v_*/v_e$ , these quantities are given by

$$\Delta x_m = \frac{v_s v_e t^2}{8s_e} \times \left[ -(2 + \sin^2 \beta) + \frac{1 + 2 \sin^2 \beta}{6s_e} v_e t - \frac{v_e^2 t^2 \sin^2 \beta}{32s_e^2} \right], \quad (19)$$

$$\Delta y_m = \frac{v_s v_e t^2 \sin \beta \cos \beta}{8s_e} \left[ 1 - \frac{v_e t}{3s_e} + \frac{v_e^2 t^2}{32s_e^2} \right], \quad (20)$$

$$d = 2s_e \left\{ 1 - \left[ 1 - \frac{v_e t}{4s_e} \right]^4 \right\}, \quad (21)$$

where

$$s_e \equiv \frac{3}{4} \left( \frac{M v_e^4}{\xi \rho_0 c^4} \right)^{1/3}. \quad (22)$$

Also, to first order in  $v_*/v_e$ , we have  $\alpha = \beta$  (i.e., the measured orientation angle is equal to the orientation angle of the ejection).

In Figure 3, we show  $d$ ,  $\alpha$ ,  $\Delta x_m$  and  $\Delta y_m$  for a model with  $v_*/v_e = 0.2$ , and for four orientation angles  $\beta = 20, 45, 70$  and  $90^\circ$ , as a function of evolutionary time  $t$ . The curves in this graph were obtained from the full equations for the positions of the clumps, which for  $v_*/v_e = 0.2$  lie very close to the first order expressions given by equations (19–21).

From Figure 3 and equations (19–21) we can draw the following conclusions which may be useful when comparing the analytic model with observations:

1. The line connecting the mean positions of coeval bipolar clumps marks the direction of motion of the source. In the examples shown in Figure 3,  $\Delta y_m / \Delta x_m \ll 1$ , indicating that the source moves along the  $x$ -axis,
2. The angle between the direction of motion of the source and the line joining the two clumps (see equation 17) is very close to the ejection angle  $\beta$  measured in the reference frame moving with the source,

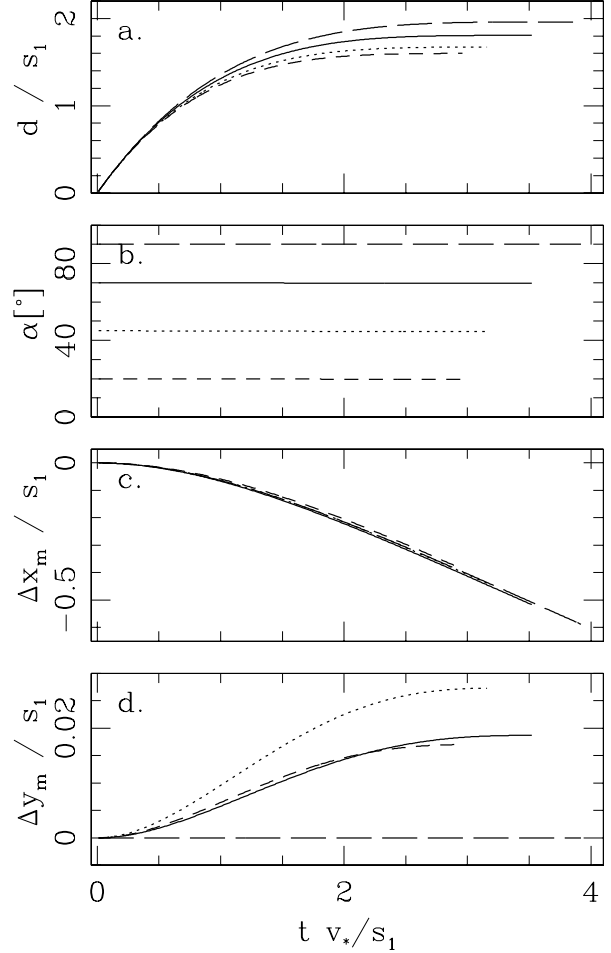


Fig. 3. **a:** Separation  $d$  between the two clumps, **b:** angle  $\alpha$  between the line joining the two clumps and the  $x$ -axis, **c** and **d:** position of the mid-point between the two clumps as a function of time, for models with  $v_*/v_e = 0.2$  and ejection directions  $\beta_1 = 20$  (short dashes),  $45$  (dotted lines),  $70$  (solid lines) and  $90^\circ$  (long dashes). The dimensionalizations of the time and distances are described in the text.

3. The behavior of the distance separating two coeval bipolar clumps as a function of time does not depend strongly on either the velocity of the source or the ejection direction.

### 3. NUMERICAL SIMULATIONS

In order to check the applicability of the analytic model described in § 2, we have computed 3D numerical simulations of a bipolar ejection of two clumps from a source embedded in a moving, homogeneous environment. We start from the initial condition shown in Figure 4. Two homogeneous, spherical clumps of radius  $r_c$  are located on the  $xy$ -plane,

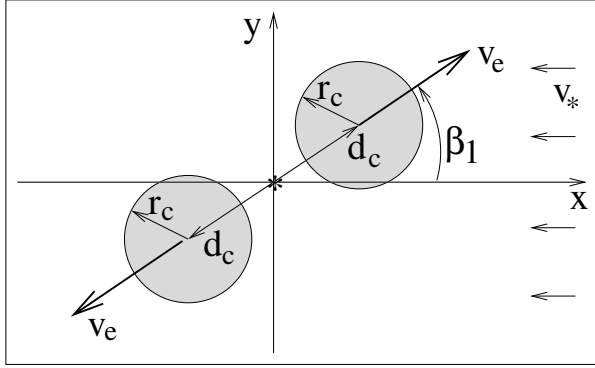


Fig. 4. Schematic diagram of the initial configuration used for the numerical simulations. In a frame of reference moving with the outflow source (located at the origin), the environment flows with a velocity  $v_*$  in the  $-x$ -direction. Two spherical clumps (of initial radius  $r_c$ ) are located at a distance  $d_c$  from the source, travelling in opposite directions with a velocity  $v_e$  along a line which lies on the  $xy$ -plane and makes an angle  $\beta_1$  with respect to the  $x$ -axis.

on an axis placed at an angle  $\beta$  with respect to the  $x$ -axis. The clumps move along this axis with a velocity  $v_e$ , and their centers are situated at a distance  $d_c$  from the origin at  $t = 0$ . The surrounding environment is homogeneous, and initially moves in the  $-x$ -direction with a velocity  $v_*$  (this flow is maintained at all times as an inflow condition in the  $+x$  boundary of the computational domain).

We run two 3D simulations with identical parameters:  $r_c = 5 \times 10^{15}$  cm,  $d_c = 1.2r_c$ ,  $\beta = 45^\circ$  and  $v_e = 100$  km s $^{-1}$ . The clumps have an initial density  $n_c = 15000$  cm $^{-3}$  and a temperature  $T_c = 100$  K. The environment moves with a velocity  $v_* = 50$  km s $^{-1}$ , and has a density  $n_{\text{env}} = 1000$  cm $^{-3}$  and  $T_{\text{env}} = 1000$  K. Both the clump and the environment are initially neutral (except for a seed electron density  $n_e = 10^{-4}n$  coming from singly ionised C).

The numerical integrations are carried out with the “yguazú-a” adaptive grid code, integrating the 3D gasdynamic equations and a single rate equation for the ionization of H. A parametrized cooling function (calculated as a function of the temperature, the density and the H ionisation fraction) is included in the energy equation. The version of the code that is used is identical to the one described in detail by Raga et al. (2007), who studied the propagation of a single, dense clump.

A computational domain of size  $(3.0, 3.0, 1.5) \times 10^{17}$  cm (along  $x, y, z$ ) with an inflow condition in the  $+x$  boundary (and outflow conditions on all of the other boundaries) was used. The outflow source

(i.e., the position of the origin of the coordinate system shown in Figure 4) lies on the center of the  $y$ - and  $z$ -extent of the computational domain, and at a distance of  $2.0 \times 10^{17}$  from the left boundary along the  $x$ -axis of the domain.

We have carried out two simulations with identical setups. The only difference between the two simulations is the resolution. In our low resolution simulation, we have a 5-level, binary adaptive grid with a maximum resolution (along the three axes) of  $1.17 \times 10^{15}$  cm, corresponding to a uniform grid simulation (at the maximum resolution of the adaptive grid) of  $256 \times 256 \times 128$  points. The high resolution simulation has an extra grid level, with a resolution of  $5.86 \times 10^{14}$  cm. Therefore, the diameter of the bullets is resolved with  $\approx 8$  and 17 points in the low and high resolution simulations (respectively). Our best resolution is therefore a factor of  $\sim 10$  lower than the one of the bullet simulations of Raga et al. (2007).

In Figure 5, we show a time-sequence of the density stratifications on the central  $xy$ -plane of the simulations (this plane includes the velocity of the streaming environment and the ejection axis). We see that both simulations give qualitatively similar results. At the later evolutionary times, the two clumps travel to distances from the source  $\sim 5\%$  larger in the high resolution simulation than in the low resolution simulation. This difference can be considered as an estimate of the error in the resulting clump positions.

In Figure 5, we also show the clump positions resulting from our analytic model (see § 2). From the parameters of the simulations, we can in principle compute the values of  $\theta$  (equation 4),  $v_0$  (equation 3) and  $s_0$  (equation 6) of the corresponding analytic models for each of the two clumps. However, to do this we need an estimate of the sound speed  $c$  (see equation 6) of the neutral clumps.

In our numerical simulation, we do not directly control the sound speed of the material that has gone through a “cloudlet shock” in order to enter the “cometary phase” of the model of De Young & Axford (1967). The radiative cooling term included in our simulations results in a post-cooling region temperature of  $\sim 10^4$ , which for a neutral gas of mean molecular weight 1.3 (for a mixture of 90% H and 10% He) corresponds to an isothermal sound speed of  $\sim 8.0$  km s $^{-1}$ .

In Figure 5 we show the positions obtained from the analytic model (from equations 13 and 14, adding the appropriate offsets corresponding to the initial positions of the clumps) for two isothermal sound speeds:  $c = 7$  (with “ $\times$ ”) and 9 km s $^{-1}$  (with

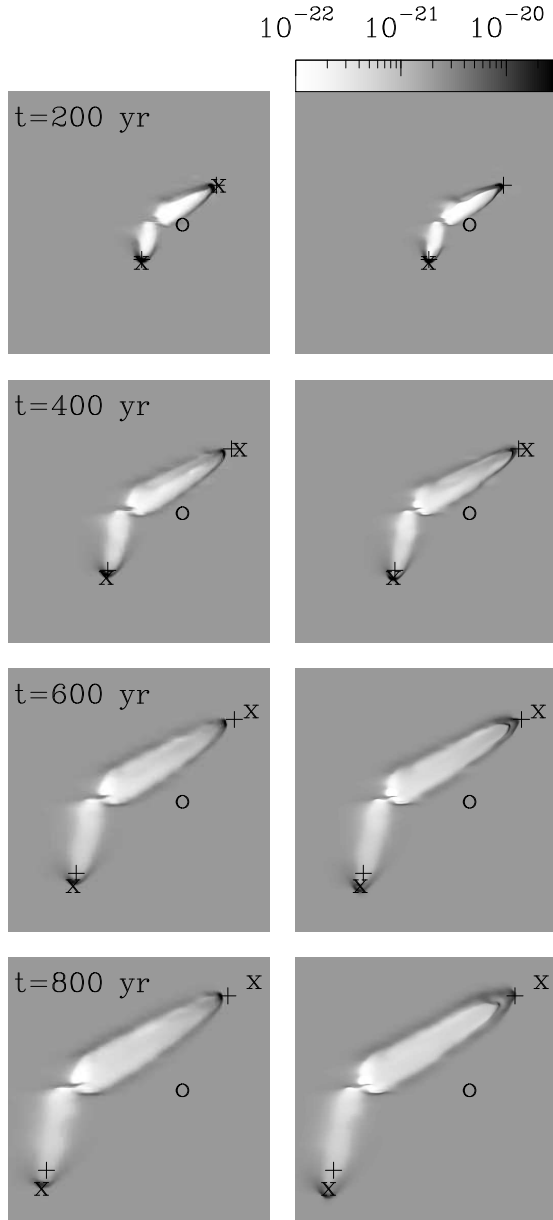


Fig. 5. Density stratifications on the  $xy$ -plane (i.e., the mid-plane of the ejection) for different integration times (given on the top of the left plots) for the low (left) and the high resolution (right) simulations. The open circle shows the position of the outflow source (which does not move in the reference system of the simulation). The positions of the condensations obtained from the analytic model are shown for an assumed isothermal sound speed  $c = 7 \text{ km s}^{-1}$  (with “ $\times$ ”) and for  $c = 9 \text{ km s}^{-1}$  (with “ $+$ ” symbols). The displayed domains have a physical size of  $(3, 3) \times 10^{17} \text{ cm}$ . The densities are given with the logarithmic greyscale shown at the top right (in  $\text{g cm}^{-3}$ ). The parameters of the simulations are described in the text.

“ $+$ ”). We see that the positions of the clump on the top half of the simulation agree better with the  $c = 9 \text{ km s}^{-1}$  model, and the positions of the bottom clump agree better with the  $c = 7 \text{ km s}^{-1}$  analytic model. This result is qualitatively consistent with the fact that the top clump (which travels against the environmental flow) has larger shock velocities than the bottom clump, so that higher average temperatures of the shocked clump material might be expected.

#### 4. CONCLUSIONS

We have presented an analytic model (§ 2) describing the motion of a bipolar clump ejection from a source in relative motion with respect to the surrounding environment. From the analytic model, we obtain simple recipes for calculating the clump trajectories as a function of time, and also for deriving some of the parameters of the ejection from observations of clumps in HH flows.

In particular, we find that to first order in  $v_*/v_e$  (where  $v_*$  is the velocity of the outflow source with respect to the environment, and  $v_e$  is the ejection velocity), the mean position obtained with the positions of two coeval clumps (ejected in a single, bipolar ejection event) always lies on the axis defined by the motion of the outflow source. Also, the orientation of the line joining the two coeval clumps points in the direction in which the two clumps were ejected (again to first order in  $v_*/v_e$ ). Finally, the distance between the two coeval bipolar clumps as a function of time does not depend strongly on either the ejection direction or the velocity of the source. For a typical HH ejection in which the motion of the source is at most  $v_* \sim 10 \text{ km s}^{-1}$  and  $v_e \sim 100 \text{ km s}^{-1}$ , these simple predictions are clearly applicable.

We have also compared our analytic solution with 3D simulations of a bipolar clump ejection. We have studied only a single parameter set, but we present two simulations at different resolutions. We find that though the details of the clump evolution differ, the positions of the clumps (as a function of time) agree well at the two resolutions. We have compared the clump positions with the predictions of the analytic model, and again find a reasonably good agreement. From this comparison, we conclude that the analytic model can quite safely be used to interpret observations of bipolar HH object ejections from moving sources.

JC and AR acknowledge support from the DGAPA-UNAM grant IN108207, from the Conacyt grants 46828-F and 61547, and from the “Macroproyecto de Tecnologías para la Universidad de la

Información y la Computación” (Secretaría de Desarrollo Institucional de la Universidad Nacional autónoma de México).

## REFERENCES

- Bally, J., & Reipurth, B. 2001, *ApJ*, 546, 299  
Cabrit, S., & Raga, A. C. 2000, *A&A*, 354, 667  
Cantó, J., Espresate, J., Raga, A. C., & D’Alessio, P. 1998, *MNRAS*, 296, 1041  
Cantó, J., & Raga, A. C. 1995, *MNRAS*, 277, 1120  
Ciardi, A., Ampleford, D. J., Lebedev, S. V., & Stehle, C. 2008, *ApJ*, 678, 968  
De Young, D. S., & Axford, W. I. 1967, *Nature*, 216, 129  
Goodman, A. A., & Arce, H. G. 2004, *ApJ*, 608, 831  
Lim, A. J., & Raga, A. C. 1998, *MNRAS*, 298, 871  
Masciadri, E., & Raga, A. C. 2001, *ApJ*, 121, 408  
Raga, A. C., Esquivel, A., Riera, A., & Velázquez, P. F. 2007, *ApJ*, 668, 310

- J. Cantó: Instituto de Astronomía, Universidad Nacional Autónoma de México, Apdo. Postal 70-264, 04510 México, D. F., Mexico.  
L. Loinard and L. F. Rodríguez: Centro de Radioastronomía y Astrofísica Teórica, Universidad Nacional Autónoma de México, Apdo. Postal 3-72 (Xangari), 58089 Morelia, Michoacán, México (l.loinard, l.rodriguez@astrosmo.unam.mx).  
A. C. Raga: Instituto de Ciencias Nucleares, Universidad Nacional Autónoma de México, Apdo. Postal 70-543, 04510 México, D. F., Mexico (raga@nucleares.unam.mx).